PHYSICAL REVIEW A **88**, 011801(R) (2013)

Loss and gain signals in broadband stimulated-Raman spectra: Theoretical analysis

Upendra Harbola and Siva Umapathy
Inorganic and Physical Chemistry, Indian Institute of Sciences, Bangalore, Karnataka 560012, India

Shaul Mukamel
Department of Chemistry, University of California, Irvine, California 92697-2025, USA

(Received 6 October 2012; published 2 July 2013)

Stimulated optical signals obtained by subjecting the system to a narrow band and a broadband pulse show both gain and loss Raman features at the red and blue side of the narrow beam, respectively. Recently observed temperature-dependent asymmetry in these features [Mallick *et al.*, J. Raman Spectrosc. **42**, 1883 (2011); Dang *et al.*, Phys. Rev. Lett. **107**, 043001 (2011)] has been attributed to the Stokes and anti-Stokes components of the third-order susceptibility, $\chi^{(3)}$. By treating the setup as a steady state of an open system coupled to four quantum radiation field modes, we show that Stokes and anti-Stokes processes contribute to both the loss and gain resonances. $\chi^{(3)}$ predicts loss and gain signals with equal intensity for electronically off-resonant excitation. Some asymmetry may exist for resonant excitation. However, this is unrelated to the Stokes vs anti-Stokes processes. Any observed temperature-dependent asymmetry must thus originate from effects lying outside the $\chi^{(3)}$ regime.

DOI: 10.1103/PhysRevA.88.011801 PACS number(s): 42.65.Dr, 42.65.Re, 82.37.Vb, 78.47.nj

Nonlinear optical spectroscopy [1] is commonly used to study the dynamics and the microscopic structure of molecules and crystals. The nonlinear response of matter is generated by multiple interactions with the radiation fields and contains useful information that is encoded in the form of resonances in the response. Raman resonances are obtained when the difference of two field frequencies coincides with a low-frequency transition of matter. Nonlinear Raman techniques, such as coherent anti-Stokes Raman spectroscopy (CARS) and stimulated Raman scattering (SRS), have been widely applied for material characterization and biomedical imaging [2–5]. Spontaneous Raman signals are positive whereas stimulated (heterodyne-detected) Raman processes give both positive (gain) and negative (loss) peaks. We consider the experiment shown in Fig. 1, whereby a femtosecond broadband pulse and a picosecond narrow pulse interact simultaneously with the molecule to generate the signal [6,7].

The loss and the gain features in the transmission of the broadband pulse are observed on the blue (high-frequency, $\omega_H > \omega_P$) side and the red (low-frequency, $\omega_L < \omega_P$) side of the picosecond pulse (frequency ω_P), respectively [8]. An asymmetry in the loss and gain signal intensities was observed by Dang *et al*. [9] and attributed to the Stokes and anti-Stokes components of the third-order optical susceptibility, $\chi^{(3)}$ [10]. Such temperature-dependent asymmetry, anti-Stokes/Stokes $\sim e^{-\omega_0/k_B T}$, where ω_0 is the Raman vibrational resonance, and T and k_B are the absolute temperature and the Boltzmann constant, respectively, is well established in spontaneous Raman. However, in this Brief Report we show that the spontaneous Raman analogy does not apply to broadband stimulated Raman processes. Using a quantum treatment of the radiation field we show that both Stokes and anti-Stokes processes contribute to the stimulated signals at ω_H and at ω_L. In fact, for an off-resonant excitation, the loss and gain intensities are identical. The interpretation of Dang *et al*. of their experimental result based on the theory of Ref. [10] is thus incorrect. The origin of the symmetry becomes clear by looking at the setup as nonequilibrium steady state with energy exchange among various field modes, with conservation of field energy. $\chi^{(3)}$ contains all the relevant information about the third-order response of the molecule. Although it is immaterial whether $\chi^{(3)}$ is computed semiclassically or quantum mechanically, we note that the semiclassical calculation treats the signal mode in a classical macroscopic fashion, unlike the other three modes, which breaks the symmetry and obscures the physics. The quantum approach, on the other hand, treats the entire process as a nonequilibrium steady state with all modes treated equally. The underlying symmetries and energy conservation are clearly revealed and become obvious in the quantum formulation. The loss-gain symmetry may be violated for electronically resonant excitation. However, this is unrelated to the Stokes–anti-Stokes asymmetry but rather depends on accidental resonances and is influenced by the excited-state lifetime.

We consider a Raman process as shown in Fig. 1 in a molecule with vibrational frequency ω_0. The Raman resonances in this setup are at the frequencies $\omega_H = \omega_P + \omega_0$ and $\omega_L = \omega_P - \omega_0$. There are three relevant modes: high (ω_H), low (ω_L), and ω_P is intermediate.

The Hamiltonian is given by

$$H = H_m + H_f + H_{\rm int}, \tag{1}$$

where ($\hbar = 1$), $H_m = \sum_{a=g,g',e,e'} \omega_a |a\rangle\langle a|$, and $H_f = \sum_{i=L,P,H} \omega_i a_i^\dagger a_i$ are the noninteracting molecular and field Hamiltonians, respectively, and

$$H_{\rm int}(t) = \sum_{i=L,P,H} \sum_{a\neq b} (A_i a_i e^{-i\omega_i t} \mu_{ab} B_{ab}^\dagger + \text{H.c.}) \tag{2}$$

represents the interaction of the radiation field with the molecule, where $B_{a,b}^\dagger = |b\rangle\langle a|$ is the exciton operator with $|a\rangle$ and $|b\rangle$ representing the many-body states of the molecular system, and μ_{ab} is the transition dipole matrix element between

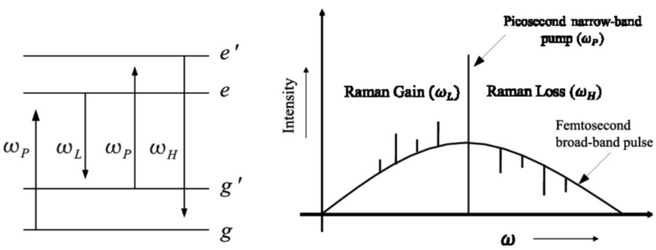

FIG. 1. Left panel: Molecular level scheme. g,g' represent vibrational states corresponding to the ground electronic state, while e,e' correspond to the electronic excited state. Right panel: Power spectrum of the fields in a stimulated Raman process generated by a broadband and a narrow-band pulse. The Raman gain and loss signals appear on the low- (red), ω_L, and the high- (blue), ω_H, frequency sides of the picosecond narrow pump pulse, respectively. Both Stokes and anti-Stokes processes contribute to the loss and gain signals (see text).

states $|a\rangle$ and $|b\rangle$. $A_j = (2\pi\omega_j/\Omega)^{1/2}$ is the field amplitude, with Ω representing the quantization volume.

The net rate of change of photon number in the jth mode of the radiation field is given by

$$S_j = \frac{d}{dt}\langle a_j^\dagger a_j\rangle = -i\big(S_j^{(1)} - S_j^{(2)}\big), \tag{3}$$

with

$$S_j^{(1)} = A_j\mu_{ba}^*\langle \hat{a}_{jL}^\dagger(t)\hat{B}_{abL}(t)\rangle, \tag{4}$$

$$S_j^{(2)} = A_j\mu_{ba}\langle \hat{a}_{jL}(t)\hat{B}_{abL}^\dagger(t)\rangle, \tag{5}$$

where $\hat{a}_L$ and $\hat{B}_{abL}$ are Liouville space operators [11].

We assume that the radiation field is initially in a coherent state $|F\rangle = A_0\exp\{\sum_j f_j a_j^\dagger\}|0\rangle$, where $|0\rangle$ represents the vacuum state, $a_j|F\rangle = f_j|F\rangle$, and $A_0 = \exp\{\sum_j |f_j|^2\}$ is the normalization constant. The average number of photons for the jth mode in the coherent field is $\langle F|a_j^\dagger a_j|F\rangle = |f_j|^2$.

For the molecular level scheme shown in Fig. 1, the lowest-order signal is generated by the third-order susceptibility induced by the external fields. We therefore need to compute the correlation functions in Eq. (4) to third order in H_{int}. This is done using a superoperator representation and loop diagrams [11,12].

Traditionally, the nonlinear susceptibility is calculated using the semiclassical theory that treats all fields as classical. The signal mode is calculated macroscopically by solving Maxwell's equations. This breaks the symmetry and obscures the analysis. By treating all field modes quantum mechanically, the process is viewed as nonequilibrium steady state with respect to the energy exchange between the high- and low-frequency modes. All incident modes as well as the signal modes are treated on the same footing. We assume that the molecule is initially in thermal equilibrium with probability P_g to be in state $|g\rangle$. Interaction with the radiation fields induces Raman transitions between states $|g\rangle$ and $|g'\rangle$.

The processes that change the field intensity at mode ω_H are represented diagrammatically in Fig. 2. Diagrams (1)–(4) correspond to $S^{(1)}$, while (1′)–(4′) give $S^{(2)}$.

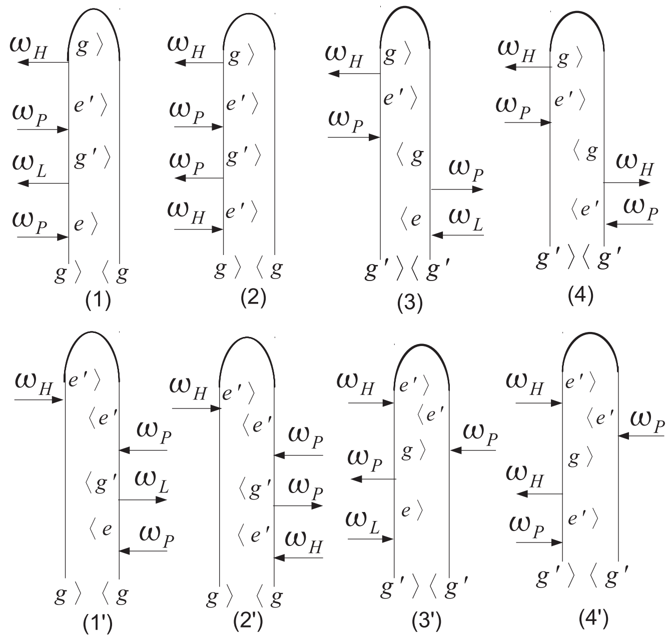

FIG. 2. The eight contributions to the stimulated Raman signal at the high-frequency mode, ω_H. Diagrams (1),(2),(1′),(2′) represent Stokes processes and lead to a *loss* in the ω_H intensity, while diagrams (3),(4),(3′),(4′) represent anti-Stoke processes and lead to a *gain* in the ω_H intensity. The net signal is the difference of the two processes.

Using the rules given in Ref. [13], we obtain the following expressions for diagrams (1)–(4) [$S^{(1)} = S_1 + S_2 + S_3 + S_4$]:

$$S_1(-\omega_H,\omega_P,-\omega_L,\omega_P) = \frac{P_g}{6}\sum_{e,e'}\frac{\mu_{ge}\mu_{g'e}^*\mu_{g'e'}\mu_{ge'}^*\epsilon_L^*\epsilon_H^*\epsilon_P^2}{(\omega_P-\omega_{eg}+i\eta)^2(\omega_H-\omega_P-\omega_{g'g}+i\eta)}, \tag{6}$$

$$S_2(-\omega_H,\omega_P,-\omega_P,\omega_H) = \frac{P_g}{6}\sum_{e'}\frac{|\mu_{ge'}|^2|\mu_{g'e'}|^2|\epsilon_H|^2|\epsilon_P|^2}{(\omega_H-\omega_{e'g}+i\eta)^2(\omega_P-\omega_L-\omega_{g'g}+i\eta)}, \tag{7}$$

$$S_3(-\omega_H,\omega_P,\omega_P,-\omega_L) = -\frac{P_{g'}}{6}\sum_{e,e'}\frac{\mu_{ge}\mu_{g'e}^*\mu_{g'e'}\mu_{ge'}^*\epsilon_L^*\epsilon_H^*\epsilon_P^2}{((\omega_P-\omega_{eg})^2+\eta^2)(\omega_P-\omega_L-\omega_{g'g}+i\eta)}, \tag{8}$$

$$S_4(-\omega_H,\omega_P,-\omega_H,\omega_P) = -\frac{P_{g'}}{6}\sum_{e'}\frac{|\mu_{ge'}|^2|\mu_{g'e'}|^2|\epsilon_H|^2|\epsilon_P|^2}{((\omega_H-\omega_{e'g})^2+\eta^2)(\omega_H-\omega_P-\omega_{g'g}+i\eta)}. \tag{9}$$

Here ϵ_j is the average complex field amplitude and the radiation field is $\epsilon_j + \epsilon_j^*$. The factor $P_g = [1 + e^{\beta(E_g - E_{g'})}]^{-1}$, where $\beta = 1/(k_B T)$, represents the thermal occupation of the ground state. Diagrams (1′)–(4′) give the complex conjugates of $S_1 - S_4$, respectively. The four components of the

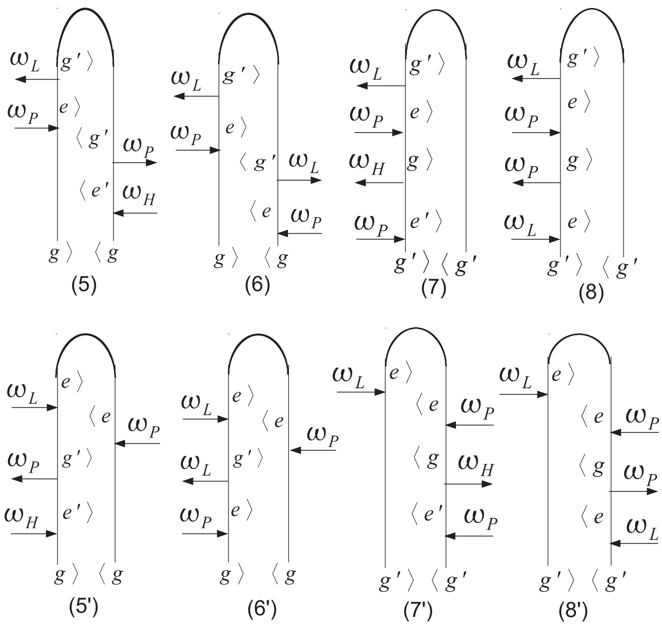

FIG. 3. The eight contributions to the stimulated Raman signal at the low-frequency mode (ω_L). Diagrams (5),(6),(5′),(6′) represent Stokes processes and lead to a *gain* in the ω_L intensity, while (7),(8),(7′),(8′) represent anti-Stokes processes and lead to a *loss* in the ω_L intensity. The net signal is the difference of the two processes.

susceptibility, $\chi_\nu^{(3)}, \nu = 1,2,3,4$, are obtained from Eqs. (6)–(9) by dropping the field amplitudes. $\chi_1^{(3)}$ and $\chi_2^{(3)}$ both contribute to the Stoke processes but generate signals in different directions, $|2k_P - k_L|$ and $|k_H|$, respectively. Similarly, $\chi_3^{(3)}$ and $\chi_4^{(3)}$ contribute to the anti-Stoke processes and generate a signal in directions $|2k_P - k_L|$ and $|k_H|$, respectively. We assume a collinear geometry where all the signals are generated in the same direction and the net signal is given as the sum of all diagrams, $S(\omega_H) = 2\,\mathrm{Im}\{\sum_{i=1}^4 S_i(\omega_H)\}$, where $\mathrm{Im}\{A\}$ denotes the imaginary part of A.

Similarly, the eight processes that contribute to the lower frequency resonance (ω_L) are given in Fig. 3. Diagrams (5)−(8) give

$$S_5(-\omega_L,\omega_P,\omega_P,-\omega_H) = \frac{P_g}{6}\sum_{e,e'}\frac{\mu_{ge}\mu^*_{g'e}\mu^*_{ge'}\mu_{g'e'}\epsilon^*_L\epsilon^2_P\epsilon^*_H}{[(\omega_P-\omega_{eg})^2+\eta^2](\omega_H-\omega_P-\omega_{g'g}-i\eta)}, \tag{10}$$

$$S_6(-\omega_L,\omega_P,\omega_L,-\omega_P) = \frac{P_g}{6}\sum_{e}\frac{|\mu_{ge}|^2|\mu_{g'e}|^2|\epsilon_L|^2|\epsilon_P|^2}{[(\omega_P-\omega_{eg})^2+\eta^2](\omega_P-\omega_L-\omega_{g'g}-i\eta)}, \tag{11}$$

$$S_7(-\omega_L,\omega_P,-\omega_H,\omega_P) = -\frac{P_{g'}}{6}\sum_{e,e'}\frac{\mu_{ge}\mu^*_{g'e}\mu^*_{ge'}\mu_{g'e'}\epsilon^*_L\epsilon^2_P\epsilon^*_H}{(\omega_P-\omega_{eg}+i\eta)^2(\omega_H-\omega_P-\omega_{g'g}-i\eta)}, \tag{12}$$

$$S_8(-\omega_L,\omega_P,-\omega_P,\omega_L) = -\frac{P_{g'}}{6}\sum_{e}\frac{|\mu_{ge}|^2|\mu_{g'e}|^2|\epsilon_L|^2|\epsilon_P|^2}{(\omega_L-\omega_{eg'}+i\eta)^2(\omega_P-\omega_L-\omega_{g'g}-i\eta)}. \tag{13}$$

Diagrams (5′)−(8′) in Fig. 3 simply yield the complex conjugates of $S_5 - S_8$. The net signal in a collinear setup is then given by $S(\omega_L) = 2\,\mathrm{Im}\{\sum_{i=5}^8 S_i(\omega_L)\}$.

For electronically off-resonant excitation, $\omega_P - \omega_{eg} \gg \eta$, where η is a lifetime broadening of the excited state, and the net signal at the lower (ω_L) and higher (ω_H) frequencies to second order in ω_p is given by

$$S(\omega_L) = \frac{P_g - P_{g'}}{3}\,\mathrm{Im}\left\{\frac{1}{\omega_P-\omega_L-\omega_{g'g}-i\eta}\times\sum_e\left[\frac{|\mu_{ge}|^2|\mu_{g'e}|^2|\epsilon_H|^2|\epsilon_P|^2}{(\omega_P-\omega_{eg})^2} + \sum_{e'}\frac{\mu_{ge}\mu^*_{ge'}\mu^*_{g'e}\mu_{g'e'}\epsilon^*_L\epsilon^2_P\epsilon^*_H}{(\omega_P-\omega_{eg})^2}\right]\right\}, \tag{14}$$

where we have used the energy conservation, $\omega_H - \omega_P = \omega_P - \omega_L = \omega_{g'g}$. The signal $S(\omega_H)$ is given by the same expression as in (14) by changing the sign of η. We thus obtain $S(\omega_H) = -S(\omega_L)$. Thus in an off-resonant third-order process, the net gain in the lower-frequency mode is identical to the net loss at the higher-frequency field modes.

Assuming that all field amplitudes and dipole matrix elements are real, Eq. (14) can be further expressed in a simpler form,

$$S(\omega_L) = \frac{P_g - P_{g'}}{3}\delta(\omega_P-\omega_L-\omega_{g'g})\sum_e\left[\frac{\mu_{g'e}\mu_{ge}\epsilon_L\epsilon_P^2}{(\omega_P-\omega_{eg})^2}\times\left(\mu_{ge}\mu_{g'e}\epsilon_L + \sum_{e'}\mu_{g'e'}\mu_{ge'}\epsilon_H\right)\right], \tag{15}$$

and $S(\omega_H)$ is obtained by changing sign and replacing $\delta(\omega_P - \omega_L - \omega_{g'g})$ with $\delta(\omega_H - \omega_P - \omega_{g'g})$.

The classification of Raman processes as either Stokes or anti-Stokes originates in spontaneous Raman where only the downward transitions (emission) are observed. In the Stokes process the molecule gains energy by moving from state $|g\rangle$ to $|g'\rangle$ and the emitted photon is red shifted with respect to the pump. In the anti-Stokes, the molecule loses energy by reverse transfer ($|g'\rangle \to |g\rangle$) and the emitted photon is blue shifted. The Stokes process is proportional to $P(g)$, whereas the anti-Stokes to $P(g')$. The ratio of the two is temperature dependent,

$$\frac{S(\text{anti-Stokes})}{S(\text{Stokes})} = \frac{P_{g'}}{P_g}. \tag{16}$$

Applying this terminology to stimulated Raman is confusing and has resulted in the errors in Ref. [9]. We shall discuss this for the ω_H signals (Fig. 2). Diagrams 2 and 2′ only involve two field modes. They represent a Stokes process in SRS. Similarly, diagrams 4 and 4′ represent an anti-Stokes SRS. Diagrams 1 and 3 involve all three modes. They represent a CARS signal generated at $2k_p - k_L$ direction. Similarly, diagrams 1′ and

$3'$ involve all three modes. They represent a coherent Stokes Raman (CSRS) signal generated at $-2k_p + k_L$ direction. In a collinear geometry all eight diagrams must be added to get the signal at ω_H. Obviously, this may not be interpreted as anti-Stokes. The same arguments hold for the ω_L signal in Fig. 3.

If we base our assignment on the temperature dependence, we reach a different conclusion. Diagrams 1, 2, $1'$, and $2'$ are proportional to $P(g)$ and can be considered Stokes, whereas 3, 4, $3'$, and $4'$ are proportional to $P(g')$ and can be considered anti-Stokes. The error in Ref. [9] comes from associating $S(\omega_H)$ with anti-Stokes and $S(\omega_L)$ with Stokes. When all 16 diagrams are taken into account, we find a complete symmetry between the loss and the gain signals. Each process contributing to the ω_H signal has a corresponding process for ω_L. $P(g)$ and $P(g')$ contribute equally to both, and the ratio of the two resonances is thus temperature independent. It is therefore incorrect to associate the signal $S(\omega_H)$ with anti-Stokes and the signal $S(\omega_L)$ with Stokes for the stimulated Raman signal, as is evident from our diagrams. The higher-frequency (ω_H) signal is affected by the Stokes and anti-Stokes processes and the same holds for the lower-frequency (ω_L) signal. The confusing Stokes and anti-Stokes terminology should be avoided altogether when discussing stimulated signals. Any observed asymmetry in the experimental signal must be induced by other processes made possible by the broadband pulse that lies beyond $\chi^{(3)}$.

U.H. acknowledges a start-up grant (Grant No. 11-0201-0591-01-412/415/433) from the Indian Institute of Science, Bangalore, India. S.U. thanks the Department of Science and Technology, India, for the support of a J. Bose fellowship. S.M. gratefully acknowledges the support of the National Science Foundation (NSF) through Grant No. CHE-1058791 and from the Chemical Sciences, Geosciences, and Biosciences Division, Office of Basic Energy Sciences, Office of Science, United States Department of Energy (DOE).

[1] S. Mukamel, *Principles of Nonlinear Optical Spectroscopy* (Oxford University Press, New York, 1995).

[2] *Coherent Raman Scattering Microscopy*, edited by J.-X. Cheng and X. S. Xie (CRC Press, Boca Raton, FL, 2012).

[3] B. G. Saar, C. W. Freudiger, J. Reichman, C. M. Stanley, G. R. Holtom, and X. S. Xie, Science **330**, 1368 (2010).

[4] D. Zhang, M. N. Slipchenko, and Ji-X. Cheng, J. Phys. Chem. Lett. **2**, 1248 (2011).

[5] A. C. W. van Rhijn, M. Jurna, A. Jafarpour, J. L. Herek, and H. L. Offerhaus, J. Raman Spectrosc. **42**, 1859 (2011).

[6] P. Kukura, D. W. McCamant, and R. A. Mathies, Ann. Rev. Phys. Chem. **58**, 461 (2007).

[7] E. Ploetz, S. Laimgruber, S. Berner, W. Zinth, and P. Gilch, Appl. Phys. B **87**, 389 (2007); S. Umapathy, B. Mallick, and A. Lakshmanna, J. Chem. Phys. **133**, 024505 (2010).

[8] S. Umapathy, A. Lakshmanna, and B. Mallick, J. Raman Spectrosc. **40**, 235 (2009); B. Mallick, A. Lakhsmanna, and S. Umapathy, *ibid.* **42**, 1883 (2011).

[9] N. C. Dang, C. A. Bolme, D. S. Moore, and S. D. McGrane, Phys. Rev. Lett. **107**, 043001 (2011).

[10] G. L. Eesley, J. Quant. Spectrosc. Radiat. Transfer **22**, 507 (1979).

[11] U. Harbola and S. Mukamel, Phys. Rep. **465**, 191 (2008).

[12] S. Rahav and S. Mukamel, Proc. Natl. Acad. Sci. USA **107**, 4829 (2010).

[13] C. A. Marx, U. Harbola, and S. Mukamel, Phys. Rev. A **77**, 022110 (2008).